Distribution of interevent avalanche times in disordered and frustrated spin systems

John Ferre,[1] Amin Barzegar,[2] Helmut G. Katzgraber,[2,3,4] and Richard Scalettar[1]
[1]*Physics Department, University of California, Davis, California 95616, USA*
[2]*Department of Physics and Astronomy, Texas A&M University, College Station, Texas 77843-4242, USA*
[3]*Microsoft Quantum, Microsoft, Redmond, Washington 98052, USA*
[4]*Santa Fe Institute, 1399 Hyde Park Road, Santa Fe, New Mexico 87501, USA*

(Received 30 August 2018; published 10 January 2019)

Hysteresis loops and the associated avalanche statistics of spin systems, such as the random-field Ising and Edwards-Anderson spin-glass models, have been extensively studied. A particular focus has been on self-organized criticality, manifest in power-law distributions of avalanche sizes. Considerably less work has been done on the statistics of the times between avalanches. This paper considers this issue, generalizing the work of Nampoothiri *et al.* [Phys. Rev. E **96**, 032107 (2017)] in one space dimension to higher space dimensions. In addition to the interevent statistics of all avalanches, we also consider what happens when events are restricted to those exceeding a certain threshold size. Doing so raises the possibility of altering the definition of time to count the number of small events between the large ones, which provides for an analog to the concept of natural time introduced by the geophysics community with the goal of predicting patterns in seismic events. We analyze the distribution of time and natural time intervals both in the case of models that include only nearest-neighbor interactions, as well as models with (sparse) long-range couplings.

DOI: 10.1103/PhysRevB.99.024411

I. INTRODUCTION

Many physical systems, when perturbed, respond in discrete jumps between metastable states. The earth's tectonic plates provide an example of such behavior in the form of earthquakes, which release a large amount of energy before being pinned again [1]. Similarly, a sheet of paper creases and tears in jerky movements, resulting in crackling sounds [2], the vortex lines of type-II superconductors depin when the electric current becomes large enough [3], and the magnetic dipoles of ferromagnets align with a changing external magnetic field in individual steps [4,5].

In these situations, and many others, the system waits in its new configuration until further changes in a driving field induce the next jump. The history of the sample is of great importance. The configuration of the system is not just a function of the instantaneous value of the drive but depends on the path followed. In this paper, we study this phenomenon from a relatively new perspective which focuses on the distribution of interevent times and how that distribution is affected by the introduction of a threshold in the definition of an event. Our goal is not only to gain additional insight into the detailed mechanism of hysteresis but also to examine the idea of *natural time* [6] in a more simple context than the geophysical applications that have mainly been considered up to now.

Klein *et al.* have suggested [1] that an alternate approach to the prediction of large earthquakes is to use as a clock the number of smaller earthquakes rather than quantifying intervals via a traditional counting of days and years. Varotsos *et al.* first introduced the term *natural time* to describe this procedure [7,8]. Recent investigations have studied this concept in complex stochastic nonlinear processes, including its use in characterizing the current state of a system as it progresses between events [9]. Investigating natural time with geophysical data is difficult owing to the absence or incompleteness of historical, and even modern, data on small earthquakes; large earthquakes are, fortunately, not excessively common. Additionally, controlled experiments are out of the question.

Here we use numerical simulations to analyze hysteresis and natural time in the context of several simple disordered and frustrated Ising spin models [10–16] exhibiting magnetic hysteresis: the three-dimensional random-field Ising model, the Sherrington-Kirkpatrick model, and the Viana-Bray model. Our key results are: (i) The distribution of interevent times between all avalanches scales with the number of lattice sites for the random-field Ising model and the Viana-Bray model but not for the Sherrington-Kirkpatrick model. (ii) The pseudogap exponent θ, which characterizes the behavior of the interevent distribution for vanishing interevent time, is zero. (iii) The addition of long-range interactions decreases the number of small interevent times but does not affect the statistics of the intervals between large events, nor do they alter θ. (iv) Despite exploring various models and parameter regimes, we fail to find a situation where the predictive capability of the natural time method is strong for spin avalanches in magnetic hysteresis. (v) By imposing a minimum avalanche size threshold, different models can be classified by their interevent distribution. (vi) Finally, at a sufficiently large minimum avalanche size threshold, the interevent time in the Sherrington-Kirkpatrick model follows a Weibull distribution with shape factor $k \sim 1$, i.e., a Poisson distribution.

The use of simulations allows us to generalize to higher dimensions a recent analytical study by Nampoothiri *et al.* [17] on the interevent time distribution of the one-dimensional random-field Ising model. The central result of that work was

the computation of the distribution of times $P(\Delta B)$ of the magnetic field change ΔB between spin avalanches. (If the magnetic field is increased at constant rate, ΔB is proportional to time.) It was found that $P(\Delta B) \sim (\Delta B)^{\theta}$ as $\Delta B \to 0$ [17], with $\theta = 0$ for the short-range ferromagnetic random-field Ising model, whereas $\theta = 0.95$ for the long-range antiferromagnetic case. Other studies of the distribution of gaps between events have been conducted in the context of amorphous solids and hard frictionless spheres [18–22]. There, when the strain γ is sufficiently increased, a corresponding stress drop follows. The distribution of gaps $\Delta\gamma$ highlights differences between the yielding and depinning processes and reveals information on mechanical stability.

The paper is structured as follows. Section II introduces the models studied, as well as the algorithmic approach and analysis methods used. In Sec. III we present results on the statistics of interevent times for all avalanches, and in Sec. IV we repeat the analysis with the introduction of an event threshold. Section V discusses the effects of additional small-world bonds between the variables, followed by a study of return point memory and concluding remarks in Sec. VII.

II. MODEL AND METHODS

We first consider the random-field Ising model (RFIM) defined by the Hamiltonian

$$\mathcal{H}_{\mathrm{RFIM}} = -J \sum_{\langle ij \rangle} S_i S_j - \sum_i h_i S_i - B \sum_i S_i. \qquad (1)$$

Here $S_i = \pm 1$ is a discrete degree of freedom at site i of a cubic lattice with N sites, and $\langle ij \rangle$ represents a sum over nearest neighbors. J is the exchange constant between nearest-neighbor sites, and units are set so that $J = 1$. Each site i is assigned a random magnetic field h_i, drawn from a Gaussian distribution

$$P(h_i) = \frac{1}{\sqrt{\pi} R} \exp\left(-h_i^2/R^2\right). \qquad (2)$$

R controls the width of the distribution and thereby the strength of the disorder. A spatially uniform field B is used to drive the hysteresis loop.

Unlike the ferromagnetic Ising model where $h_i = 0\ \forall i$, the RFIM does not exhibit ferromagnetic order in $d = 2$ (or below). As the temperature is lowered in higher space dimensions, however, a freezing transition occurs. This is followed by a ferromagnetic transition [23–27]. Here we are not concerned with these aspects of the equilibrium finite-temperature phase diagram but instead focus on the evolution of the magnetization as the external field B is sequentially changed, with dynamics defined by each spin remaining parallel to its local environment at each step, that is, effectively $T = 0$ (see below).

Typical RFIM hysteresis curves are shown in Fig. 1. From them, we can extract the size of all the individual magnetization jumps S and hence their distribution. It is well known [28] that this distribution has power-law behavior at low disorder, which we reproduce in Fig. 2. We can also extract the distribution of time (as measured by the change in external field ΔB) between events. The latter quantity has been much less studied than the former.

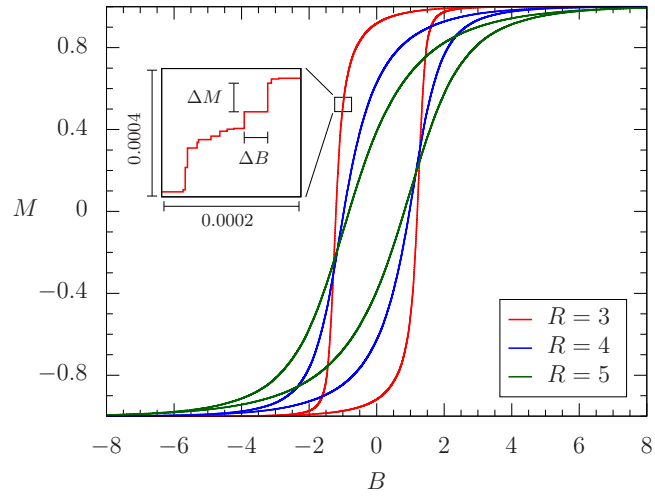

FIG. 1. Hysteresis loop of the random-field Ising model of size $N = 100^3$ with a distribution of fields of widths $R = 3$, 4, and 5. On a large scale, the curves appears to represent a smooth evolution of the magnetization $M(B)$. However, as can be seen in the inset, the magnetization $M(B)$ is composed of a series of discrete jumps. ΔM is the change in magnetization. ΔB is the interevent time.

The Sherrington-Kirkpatrick model (SKM) [29] is given by the Hamiltonian

$$\mathcal{H}_{\mathrm{SKM}} = -\sum_{i<j} J_{ij} S_i S_j - B \sum_i S_i. \qquad (3)$$

In the SKM, every site $i \in \{1, \ldots, N\}$ interacts with every other site j via J_{ij}. That is, the interaction is infinite range. The exchange constants J_{ij} are disordered, and in our study are given by a Gaussian distribution with zero mean and a standard deviation of J_0. We set $J_0 = 1$ as our unit of energy. The SKM shows self-organized criticality (SOC) for all disorder [30,31].

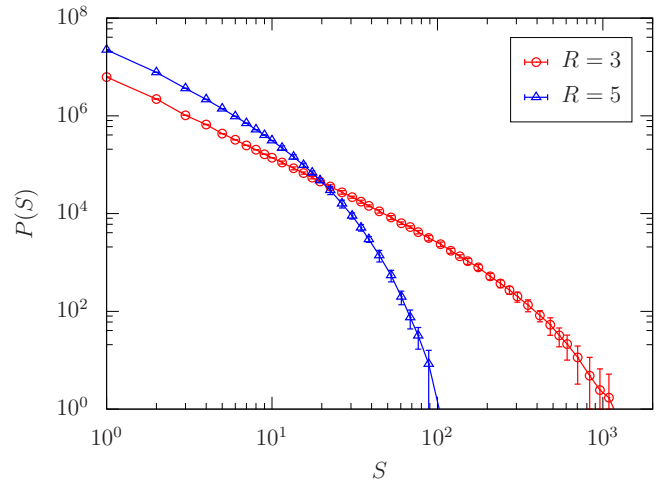

FIG. 2. Distribution of avalanche sizes for field width $R = 3$ and 5. The distribution is known to have power-law behavior for $R = R_c \approx 2.16$. A critical region, for which power law behavior persists for several decades of avalanche size, occurs up to $R \approx 4$. For details see Ref. [28].

Finally, we also study the Viana-Bray model (VBM) [32] in which each spin is randomly connected to $z = 6$ other spins. Thus, the VBM is still long ranged but with a finite coordination number. Unlike the SKM, the VBM does not have SOC [30]. Note that the RFIM has an explicit parameter R with which the disorder strength can be tuned whereas the SKM and VBM do not.

In order to generate a hysteresis loop for the RFIM, we compute the local fields,

$$B_i = -h_i - J \sum_{j \in \mathcal{N}(i)} S_j \,, \tag{4}$$

and for the SKM and VBM,

$$B_i = - \sum_{j \in \mathcal{N}(i)} J_{ij} S_j \,. \tag{5}$$

For the RFIM, $\mathcal{N}(i)$ includes the nearest neighbor spins, whereas $\mathcal{N}(i)$ for the SKM consists of all spins, while the six randomly chosen neighbors define $\mathcal{N}(i)$ for the VBM.

A hysteresis loop is generated as follows: Starting at $B = \infty$ we reduce B to a value $B_k = \max\{B_i\}$. This is the external field at which the spin S_k becomes unstable. S_k is then reversed and the reconfiguration of the lattice and of the collection of local fields $\{B_i\}$ is computed based on greedy dynamics [33]. Once S_k flips and the local fields are recomputed, the next most unstable spin l is flipped, i.e., its (updated) local field is now greater than the external field: $B_l > S_l \cdot B$. This process is continued until all unstable spins are reversed. The total count of spins flipped is recorded as the size of the associated avalanche. The avalanche size determines the change in magnetization ΔM, which is twice the total fraction of spins which flip. At this point, the external field B is reduced once again to the next largest $\{B_i\}$ and the process is repeated until all spins are flipped and the system reaches saturation but with the opposite sign of the magnetization. The interevent times are the values ΔB that the external field jumps between each completed avalanche.

We begin, in Sec. III, by analyzing the distribution of time intervals $P(\Delta B)$ which results from using the most broad definition of an avalanche, i.e., by including even the smallest possible $\Delta M = 2/N$, resulting from a single spin flip. We also calculate the pseudogap exponent θ, given by $P(\Delta B) \sim (\Delta B)^{\theta}$ as $\Delta B \to 0$. This follows the procedure described in recent literature [17] on the one-dimensional RFIM.

Next, in Sec. IV we use a minimal threshold ΔM, only above which a change in a spin configuration is considered an event. We analyze how the distribution in interevent times is affected by making $\Delta M > 2/N$. The introduction of such a threshold ΔM allows us to consider alternate measures of the *interval* between events. Specifically, we can define the *natural time* ΔA between large avalanches by counting the number of small avalanches (those with ΔM less than the threshold) which occur between large ones. We also define the *total natural time* ΔF between large avalanches to be the total number of flipped spins (i.e., the change in magnetization) which has accumulated. This latter procedure weights each small avalanche by the number of spins which turned over.

These different approaches to the interevent time are chosen to parallel analogous definitions in the geophysics community [34] where natural time employs only earthquakes exceeding a certain size as events and the number of small earthquakes between the large ones is recorded. The current state of an earthquake cycle is analyzed by constructing a cumulative distribution function of interevent times between large earthquakes, which shows a Weibull form [6],

$$f(t) = 1 - e^{-(t/\lambda)^k}. \tag{6}$$

Here λ is the scale parameter and k is the shape parameter. For $k < 1$ the cumulative probability function of the Weibull distribution has an initial rapid rise, while if $k > 1$ the initial slope is small. If $k = 1$, Eq. (6) becomes the interevent distribution of a Poisson process. The Weibull distribution is commonly used in the materials science community to characterize the time to failure, where $k < 1$ corresponds to a failure rate which decreases with time. In contrast, $k > 1$ corresponds to a failure rate which increases with time. Motivated by the geophysics problem, we perform a similar fit to the cumulative distribution of interevent times in our spin model hysteresis loops. By taking the natural logarithm of both sides twice, Eq. (6) becomes

$$\log[-\log(1 - f(t))] = k\log(t) - k\log(\lambda), \tag{7}$$

so that a plot of the data in the form $\log[-\log(1 - f(t))]$ vs $\log(t)$ yields a linear relation if $f(t)$ has a Weibull form.

III. STATISTICS OF ALL AVALANCHE INTEREVENT TIMES

We start by analyzing the distributions of time intervals that occur between every avalanche, including avalanches of a single flip, i.e., $\Delta M = 2/N$. When an avalanche occurs, we mark its magnetic field value. Then, we can define ΔB as the difference between any two consecutive avalanches and accumulate the distribution of interevent times as $P(\Delta B)$.

In order to compare distributions of different parameters properly, $P(\Delta B)$ is normalized. This is done by dividing by the total number of intervals N_{int}. As R increases to large values, the spins feel a wide range of random fields, and their local fields B_i [Eq. (4)] become widely separated. In the limit $R \to \infty$, all events become single flips because the contribution to B_i from the exchange interactions J is negligible in comparison. The total number of intervals N_{int} approaches the number of lattice sites (spins) N. Similarly, as R decreases, the total number of intervals becomes small. At $R = 0$, the hysteresis loop becomes completely square, $N_i = 1$, and the entire lattice flips from up to down at the single external field value $B = -2dJ$, where $d = 3$ is the space dimension. Normalizing $P(\Delta B)$ to N_{int} eliminates this trivial effect. The sum of all avalanches in the distribution equals unity, independent of the choice of parameters.

We begin by analyzing the RFIM, plotting the distribution of interevent times in Fig. 3. Distributions of varying lattice sizes N are seen to collapse if the event intervals ΔB are scaled by N, that is

$$P(N, \Delta B) \sim \tilde{P}(N \Delta B) \,. \tag{8}$$

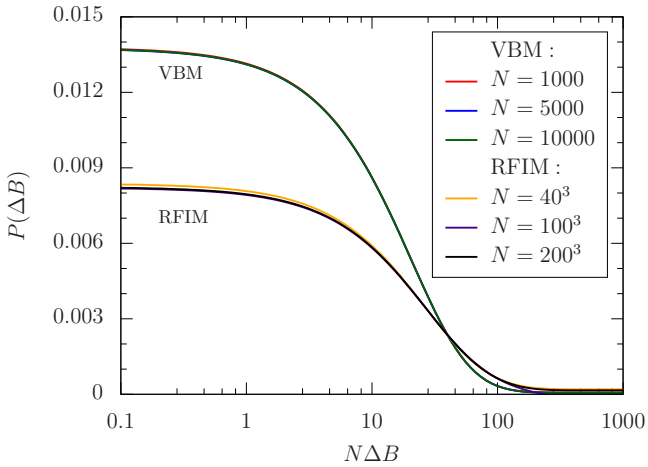

FIG. 3. Scaling collapse of the distribution of interevent times for the RFIM at field width $R = 2.3$ and the VBM for various system sizes N. If the field interval axis is scaled by N, the distributions for different N coincide. That is, $P(N, \Delta B) \sim \tilde{P}(N\Delta B)$. The vanishing slope at small ΔB indicates the pseudogap exponent defined by $P(\Delta B) \sim (\Delta B)^{\theta}$ as $\Delta B \to 0$ obeys $\theta = 0$, in agreement with analytic results in one space dimension ($d = 1$).

The interevent distribution for the VBM is similar to the RFIM (see Fig. 3) and scales with the number of variables N. Due to the fundamental difference between finite and diverging number of neighbors [30], we expect the same scaling behavior for differing finite coordination numbers of the VBM.

As can be seen in Fig. 4, the SKM distributions for different lattice sizes collapse with an *unscaled* ΔB. Other than that, the shape of the interevent distribution of all avalanches is similar to the RFIM (Fig. 3). Because the VBM is long ranged and the RFIM is short ranged, but both have similar scaling forms for $P(\Delta B)$, we conclude that the connections between distant spins do not by themselves give rise to a change from

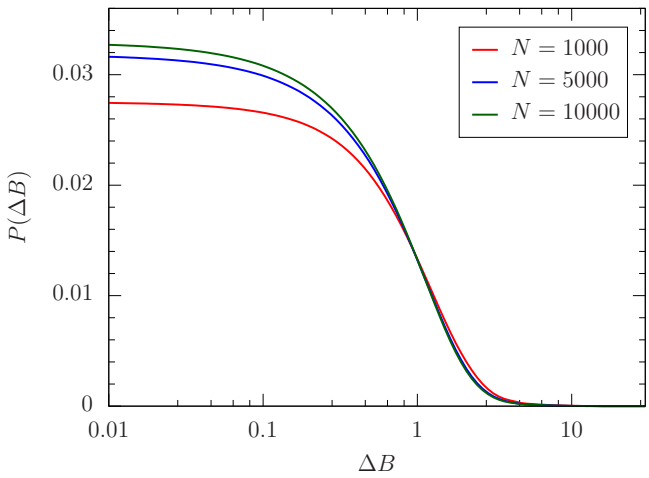

FIG. 4. Distribution of interevent times for the SKM. The distributions largely overlap, apart from a modest separation at small ΔB. In sharp contrast to the RFIM and VBM data of Fig. 3, $P(N, \Delta B)$ does not show a scaling collapse to $P(N\Delta B)$.

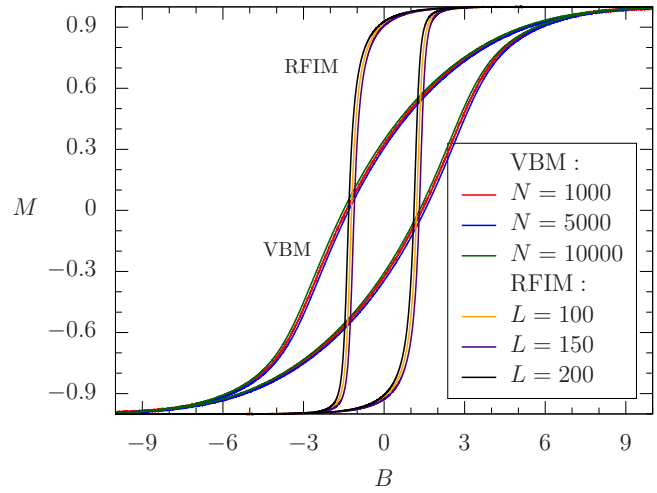

FIG. 5. Hysteresis loop for the RFIM with $R = 3$ and for the VBM for different system sizes N. The shape is similar for various lattice sizes for all disorders. As argued in the text, this independence of lattice size underlies the scaling form $P(N, \Delta B) \sim \tilde{P}(N\Delta B)$.

the RFIM collapse with $N\Delta B$. Instead, the most likely cause of scaling differences is the presence of SOC at all disorder strengths in the SKM due to the fully-connected topology.

Another way to gain insight into the scaling of interevent times is to observe the behavior of the hysteresis loops. While hysteresis loops have been extensively studied [30,35–38], we focus on the width of the loop in relation to the lattice size. For the RFIM and VBM, the loops are the same width across all lattice sizes (see Fig. 5). This means that the total time T for traversal of the loop is constant. In the limit where events are small and fairly isolated spatially, the number of events grows linearly with lattice size N, and the time ΔB between events is proportional to $1/N$. This picture offers a qualitative explanation of the dependence of P on $N\Delta B$.

The hysteresis loop for the SKM (Fig. 6) is different from the VBM and the RFIM. Its width grows as the lattice size is increased—the total time across the loop increases with N. If we again consider a limit where events are small and fairly isolated spatially, so that the number of events grows linearly with lattice size N, the interval between individual events ΔB is expected to be roughly independent of lattice size.

Returning to the RFIM, we consider the dependence of the limit of interevent time distribution at small ΔB on disorder width R. Figure 7 shows the distributions for different R values. The quantity

$$C(R) = \lim_{N\Delta B \to 0} \tilde{P}(N\Delta B) \tag{9}$$

characterizes the value of the distribution at the smallest interval sizes. The inset to Fig. 7, showing $C(R)$, exhibits a peak for $R \approx 3.7$. Note that for the analytical calculation of the one-dimensional case, $C(R)$ peaks at $R \approx 1$ [17].

The flatness of $P(\Delta B)$ as $\Delta B \to 0$ implies that the pseudogap exponent $\theta = 0$ for all R in the RFIM. It likewise vanishes for the SKM and VBM. This value for the exponent is the same as the one-dimensional RFIM [17]. It has been argued that this is a consequence of the mapping between the RFIM and a depinning process when the dimensionality

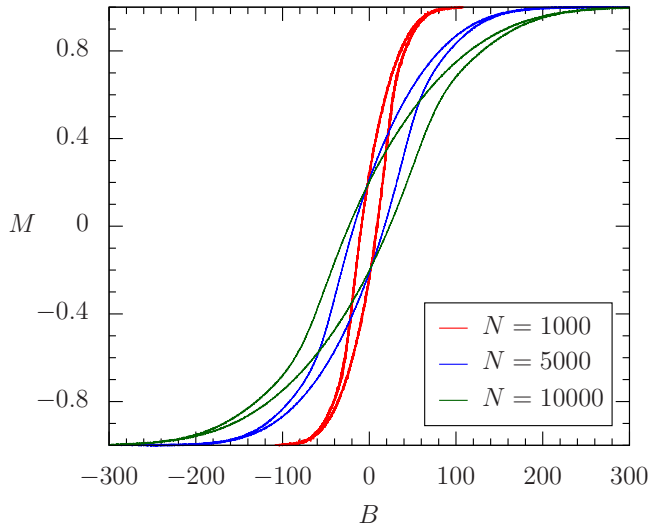

FIG. 6. Hysteresis loop for the SKM. The width of the loop (e.g., at $M = 0$) increases with lattice size: $\Delta B \sim 9$, 17, and 23 for $N = 1000$, 5000, and 10 000, respectively. As argued in the text, this dependence on lattice size underlies the difference in scaling behavior from the RFIM and VBM cases.

is less than 5 [39]. The depinning process is known to have $\theta = 0$ [18]. Thus our results confirm previous conjectures on the nature of the gap statistics.

The interevent time distributions $P(\Delta B)$ of Figs. 3 and 4 illustrate the unpredictability of avalanche occurrences. The distributions have significant weight over several orders of magnitude of ΔB. The time between avalanches, as measured by the traditional definition ΔB (which is proportional to the conventional time interval Δt if B is swept at constant rate), takes a very wide range of values. In Sec. IV we explore whether alternate definitions might yield a narrower distribution and hence more predictable intervals.

IV. STATISTICS OF ABOVE THRESHOLD INTEREVENT TIMES

In Sec. III we have seen that the distribution of interevent times $P(\Delta B)$ is very broad when all avalanches are considered as events. We now reanalyze the distribution but impose an event threshold L_A. This both eliminates the small (and therefore presumably more random) magnetization jumps and opens the door to counting the number of jumps as an alternate definition of interevent time. This latter procedure follows suggestions in the geophysics community where including an avalanche threshold was argued to help determine where a certain geographic region is located in the earthquake cycle.

In geophysics studies, the imposition of a threshold was shown to lead to the interevent distribution following a Weibull process [6]. Here we use a similar approach, and verify if the statistics obey the same distribution. We examine several definitions of the interevent time: ΔA characterizes the number of small avalanches, ΔF the total number of individual flips. This complements the use of ΔB, the change in magnetic field between events (see Sec. III).

If large avalanches tended to occur after relatively *constant* numbers of small avalanches ΔA, then a plot of the cumulative distribution function $f(\Delta A)$ would take the form of an abrupt step, reflecting a sharply peaked probability $P(\Delta A)$, i.e., large events separated by *one specific* ΔA. Figure 8 shows the cumulative distribution functions for different disorder strengths R and for different choices of the threshold L_A for counting small avalanches. We see no significant tendency for the cumulative distribution to become more steplike than when plotted as a function of ΔB.

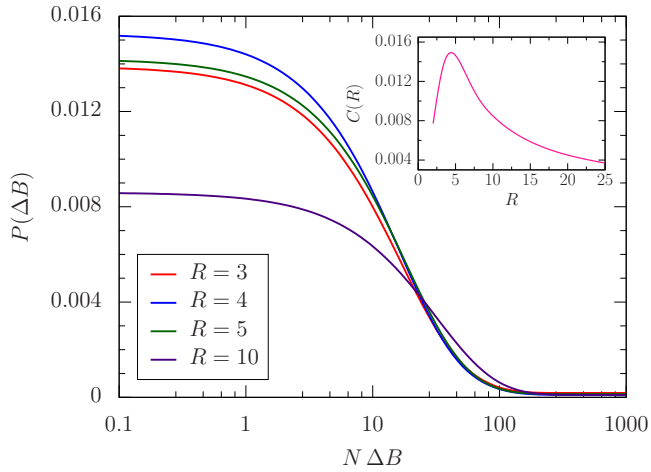

FIG. 7. Distribution of interevent times for the RFIM for various field widths R. $C(R)$ [the value of the interevent distribution at small ΔB, Eq. (9)] is highest for $R = 4$. The behavior of $C(R)$ is nonmonotonic. The slope of $P(\Delta B)$ is zero for small ΔB, confirming that $\theta = 0$ for all R. Inset: $C(R)$ [Eq. (9)] for a fine mesh of R values. This allows for a more refined determination of the peak position, $R \approx 3.7$. This is in qualitative agreement with the $d = 1$ analytical result, which has a similar peak at $R = 1$ [17].

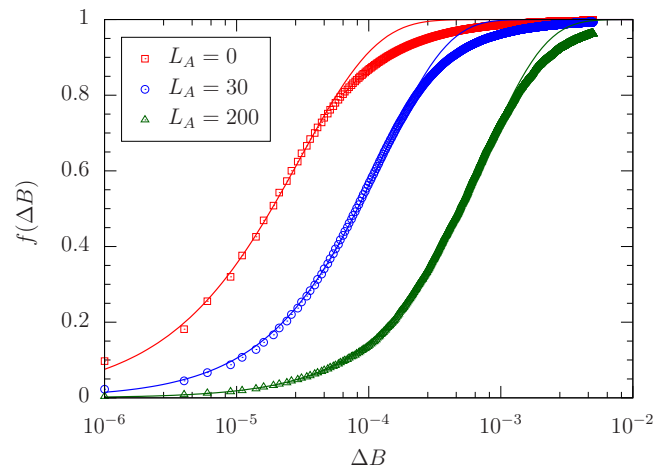

FIG. 8. Cumulative distribution of the interevent times for the RFIM at $R = 3$. The lattice size is $N = 100^3$. The data (points) are plotted along with the Weibull fit (lines). Several large avalanche thresholds are imposed. The Weibull cumulative distribution function appears to fit reasonably well to the cumulative distribution of the data. This occurs for ΔA and ΔF as well. The deviations are examined more critically in Fig. 9, which better emphasizes deviations from the Weibull form.

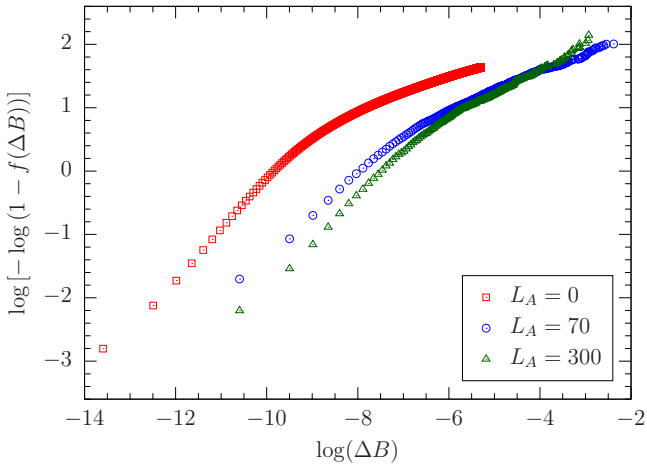

FIG. 9. Cumulative distribution of the interevent times for the RFIM at $R = 2.3$ on a double-logarithmic scale. For the distribution to be fit by a Weibull distribution, the data must be linear. Instead, the curves show a significant downward concavity for all values of L_A. The same trend is found for ΔA (not shown).

Although the continued broadness of the distributions of Fig. 8—despite the replacement of ΔB by ΔA and ΔF—suggests that natural time does not sharpen the distribution of interevent spacing, we can still ask whether the underlying distributions of interevent times are similar to those found in geophysics applications. Figure 8 shows the Weibull fits to the distributions f in addition to the raw data.

While naively it appears that the data of Fig. 8 might follow a Weibull interevent distribution, a more discerning check is made by plotting the data with modified axes: $\log[-\log(1 - f(t))]$ vs $\log(t)$. On these axes, the data should form a straight line, as discussed earlier [see Eq. (7)].

First, we analyze the RFIM, where the distributions do not appear to be well fit by a Weibull distribution by any definition of time (see Figs. 9 and 10). We focus on $R > R_c \sim 2.16$, the critical value of R below which an infinite avalanche occurs in which a macroscopic fraction of the spins all flip at once [28].

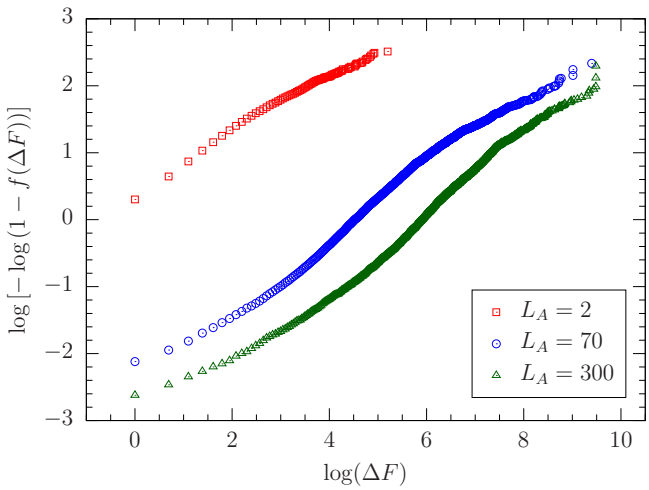

FIG. 10. Cumulative distribution of the interevent times for the RFIM at $R = 2.3$ on a double-logarithmic scale. The data are closest to linear for the smallest threshold.

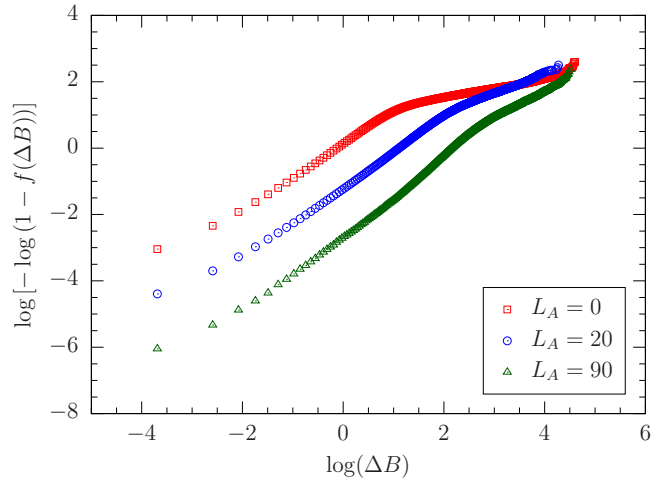

FIG. 11. Cumulative distribution of the interevent times for the SKM with lattice size $N = 10\,000$. As L_A is increased, the data become more linear, which shows that the distribution of ΔB can be approximated as Weibull at sufficiently large L_A. The slope for $L_A = 90$ is $k \sim 1$, which implies that the Weibull distribution simplifies into a Poisson distribution. The same phenomenon occurs in the VBM with a slope of $k \sim 0.8$.

Above R_c, ΔA and ΔB yield a curve that is concave down, while ΔF yields a curve with an inflection point. The fact that the distribution is concave down implies that there is a scarcity of large-time intervals for the distributions to be Weibull. The quality of the fits of RFIM interevent times ΔB to a Weibull distribution (Fig. 9) does not appear to be very sensitive to the value of the avalanche threshold. In the case of natural time ΔF (Fig. 10) smaller threshold gives a somewhat better fit. In either case, as L_A increases, the average time between events increases, which leads to a lower intercept with the vertical axis; this follows from Eq. (7). The situation is rather different for the SKM when using the interevent time ΔB. As L_A is increased, the Weibull fit improves significantly, as shown in Fig. 11. Interestingly, the shape parameter k is close to unity, i.e., the distribution is Poissonian. The same fit improvement with larger L_A occurs for the VBM (not shown), but $k \sim 0.8$ in that case. We are unable to determine if this value of k varies with the VBM's coordination number z, and we might perform simulations of varying z in a future paper. The SKM also provides interesting results for the natural time methods. $f(\Delta A)$ is rather close to a Weibull distribution for all L_A (Fig. 12). ΔF, however, provides a fit that worsens as L_A is increased. The VBM shows similar results in that both methods of natural time provide the best fit at low L_A.

V. EFFECT OF LONGER RANGE COUPLINGS

On large lattices, small avalanches amongst clusters of spins which are far from each other are likely to occur in a rather independent manner. This might be problematic for periodic large-event intervals, because avalanches which are decoupled are unlikely to provide a predictive countdown to an above-threshold event. In order to introduce a more collective behavior of the entire cubic lattice, we introduce long-range couplings by dividing the entire cubic lattice into

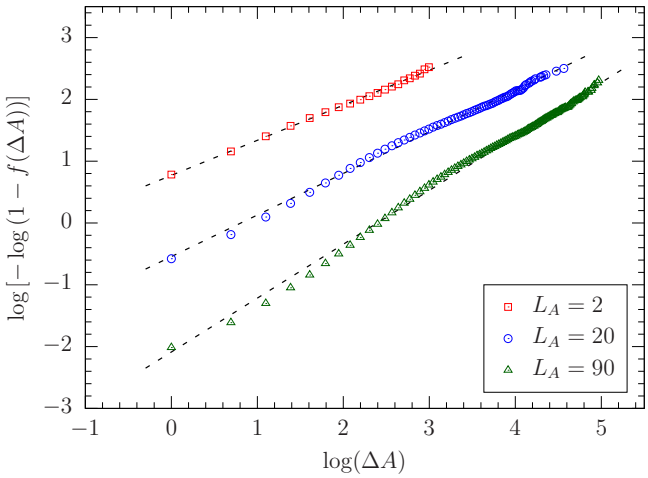

FIG. 12. Cumulative distribution of the interevent times for the SKM with lattice size $N = 10\,000$. The data are approximately linear for all L_A, i.e., the distribution is Weibull.

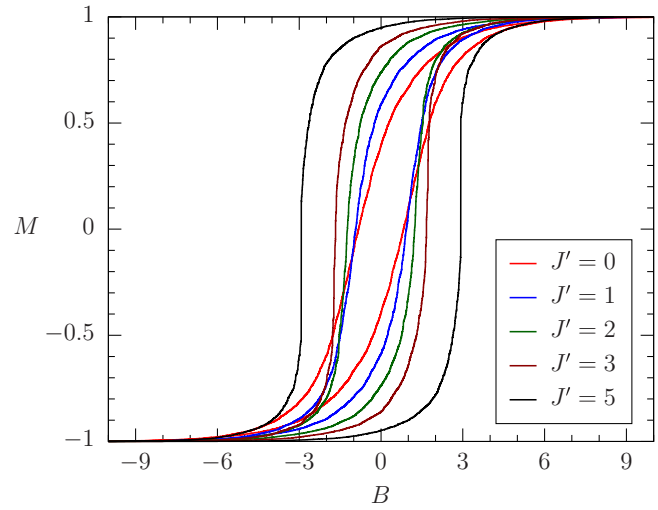

FIG. 13. Hysteresis loops for the Hamiltonian in Eq. (10) for various J' values. Here, $R = 5$, and the lattice size is $N = 30^3$. As the strength of J' is increased, the hysteresis loop becomes steeper and wider. This is due to the increased correlation of lattice sites, which causes avalanches to occur at the same magnetic field value.

randomly selected pairs of sites. At the algorithmic level, this is accomplished by starting with site 0 and then randomly selecting one of the other sites p_0 of the lattice as a partner to site 0. Note that p_0 is not allowed to be one of the existing six nearest neighbor sites. After this is done, both sites 0 and p_0 are eliminated as potential partners and one proceeds to site 1 (assuming $p_0 \neq 1$) and randomly assigns it a partner p_1. This process is continued until all sites in the cubic lattice have a seventh neighbor. When assigned in this way, the probability of a site being part of a pair is independent of the geometric proximity between the two sites (as long as they are not nearest neighbors). These longer-range neighbors are coupled by an exchange constant J', so that in the computation of the local field, and hence the determination of whether to flip S_i, Eq. (4) is generalized to include p_i as part of $\mathcal{N}(i)$. Setting $J' = 0$ recovers the original nearest neighbor only model, and increasing J' allows us, in a smooth manner, to increase the long-range interactions across the lattice. Our model Hamiltonian thus becomes

$$\mathcal{H} = -J \sum_{\langle ij \rangle} S_i S_j - J' \sum_i S_i S_{p_i} - \sum_i h_i S_i - B \sum_i S_i, \tag{10}$$

where p_i is the long-range site connected to site i. A similar procedure has previously been introduced in Ref. [40] to study finite-temperature phase transitions in Ising models with long-range interactions (which prove to be of mean-field character) and, more generally, are considered in the context of small-world networks [41].

Figure 13 shows hysteresis loops for the Hamiltonian presented in Eq. (10). The loops become steeper and the width is increased with J'. This occurs because different lattice sites become correlated, which causes avalanches to combine. The distribution of interevent times ΔB is shown in Fig. 14. For all J' values, the distribution is monotonically decreasing and larger J' values suppress the frequency of small avalanches. The pseudogap exponent is zero for any strength of the long-range connections.

$C(R)$, given by Eq. (9), is shown in Fig. 15 for different values of J'. $C(R)$ is nonmonotonic; the value of R for which $C(R)$ is largest grows with the strength of the long-range connection. The overall curve is lowered when J' is increased. As is to be expected, once the ratio of R to J' becomes large enough that the local fields dominate the system, the curves for $C(R)$ collapse.

The lowering of $C(R)$ with J' means there are fewer small interevent times for larger J' values at a given disorder R. However, despite the shift in the distribution from smaller to larger interevent times, $P(\Delta B)$ remains monotonically decreasing. These trends are present as well in Fig. 14, where the distribution becomes visibly flatter as J' is increased.

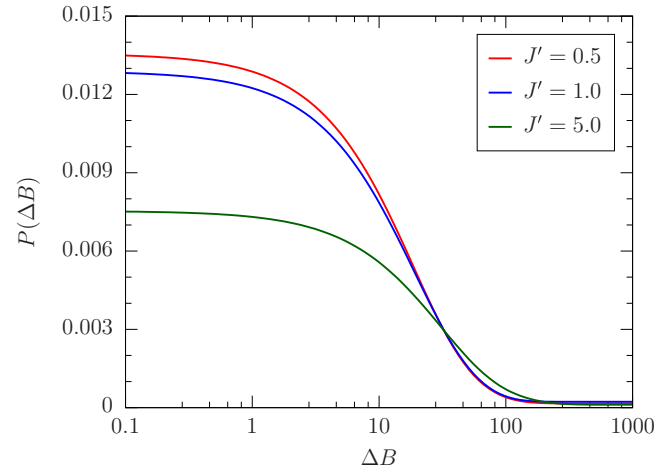

FIG. 14. Distribution of interevent times for various values of J'. The distribution is always monotonic, and there are fewer small interevent times when J' is increased. This is due to the additional correlation between avalanches.

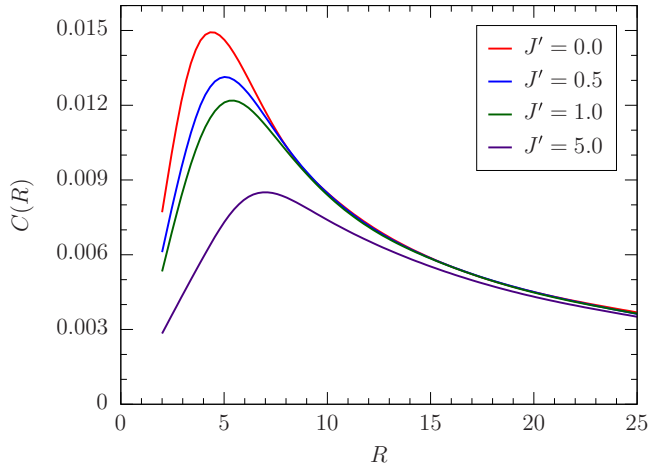

FIG. 15. $C(R)$ [Eq. (9)] plotted against the disorder strength R for various J' values. $C(R)$ is lowered as J' increases, and the curve collapses onto the $J' = 0$ case when R becomes large enough.

In order to explain this phenomenon, consider $J' = 0$ and two avalanches that occur separately in space and nearly simultaneously in time, i.e., at very similar global field value B. In this moment, the two events are uncorrelated, and they have a very small interevent time ΔB. If long-range connections are included, it is plausible that the two avalanches might now be correlated and occur simultaneously as J' grows. The probability of small avalanches decreases and of large ones increases, as seen in Fig. 16. This also implies that the frequency of small interevent times is reduced. The long-range correlations do not ever result in a peak of $P(\Delta A)$ or $P(\Delta F)$ which would indicate specific most probable *natural time spacings* which predict when a large avalanche would be imminent.

Although J' affects the quantitative value of $P(\Delta B)$, as well as $P(\Delta F)$ and $P(\Delta A)$, it does not significantly change their width. In short, the conjecture that J' might make avalanches constant in *natural time* seems to be false.

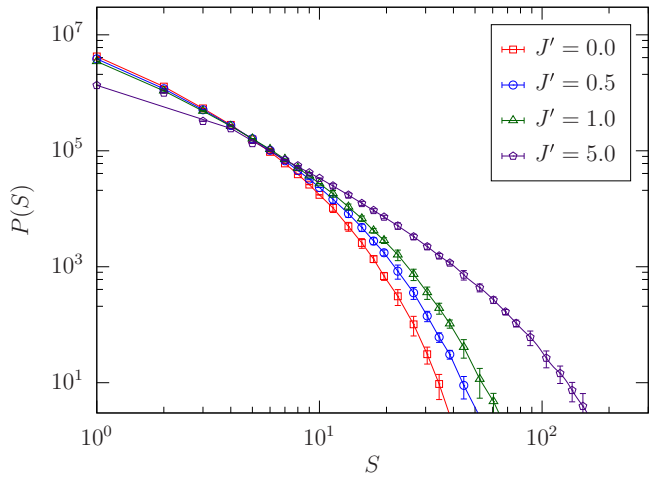

FIG. 16. Distribution of avalanche sizes plotted for various J' values for $N = 50^3$ and $R = 7$. As J' increases, there are larger avalanche sizes, and the distribution approaches the critical region, as described in Ref. [28]. This is due to the correlation of lattice sites. Note that two avalanches may occur at the same moment, which leads to a greater amount of large avalanche sizes.

VI. RETURN POINT MEMORY

In the study of hysteresis loops, "return point memory" is a central concept [42–44]. Instead of driving the system to saturation, the external field B is lowered from infinity until some intermediate field B_0 is reached. At this point, B is raised to B_1 and then lowered back to B_0, which creates an "internal" hysteresis loop. If the system exhibits return point memory (RPM), then the state (that is, the magnetization) of the system is the same at both instances of B_0.

It is natural to ask how the interevent times along an internal hysteresis loop are distributed. It is known that both the RFIM and the SKM exhibit RPM [35,42]. While the distribution of interevent times in the SKM has been shown to be well approximated by a Weibull distribution for sufficiently large L_A (see Fig. 11), the RFIM interevent times are not as well described by a Weibull distribution (see Fig. 9). Therefore, we simulate the RFIM for both $R = 2.3$ and $R = 3$ on a lattice size of $N = 200^3$ to study the interevent times for internal hysteresis loops. This helps identify whether RPM can help the RFIM interevent distributions become Weibull-like, and the results can be directly compared to Figs. 8 and 9.

The results for internal hysteresis loops are shown in Figs. 17 and 18. The data for $L_A = 0$ approach a Weibull distribution even though the data are not Weibull distributed for the smallest nonzero large avalanche. While the data in a log-log plot are not exactly linear for $R = 2.3$, there is still a striking difference between $L_A = 0$ and $L_A = 2$. A more detailed analysis on RPM is needed to fully understand the behavior of small L_A. However, we expect the same trend to occur with alternate choices of disorder and RPM turning points. Note that ΔA and ΔF are the same as the previous case when the system is driven to saturation (see Fig. 10).

VII. CONCLUSIONS

We have evaluated the distribution of interevent times of the three-dimensional random-field Ising, Sherrington-Kirkpatrick, and Viana-Bray models. Our motivation was twofold: First, to extend the analytic results for this distribution—which have been obtained in one space dimension [17]— to higher space dimensions, providing complementary numerical results to the well-studied distributions of the avalanche amplitudes. Second, to explore the idea of natural time to study if the distribution is more sharply peaked when measured by counting the number of small avalanches rather than the change in field itself.

Our conclusions regarding the first point are summarized in Figs. 3 and 4, which provide explicit forms for $P(\Delta B)$ for the different models. A central feature of our results is the scaling relation, $P(N, \Delta B) \sim \tilde{P}(N\Delta B)$ obeyed by both the RFIM and VBM, whose validity we trace to a hysteresis loop width which is nearly independent of lattice size N (Fig. 5). In contrast, the SKM hysteresis loop width changes significantly with N (Fig. 6), and $P(N, \Delta B)$ does not scale. We also observe a pseudogap exponent $\theta \approx 0$, which is the

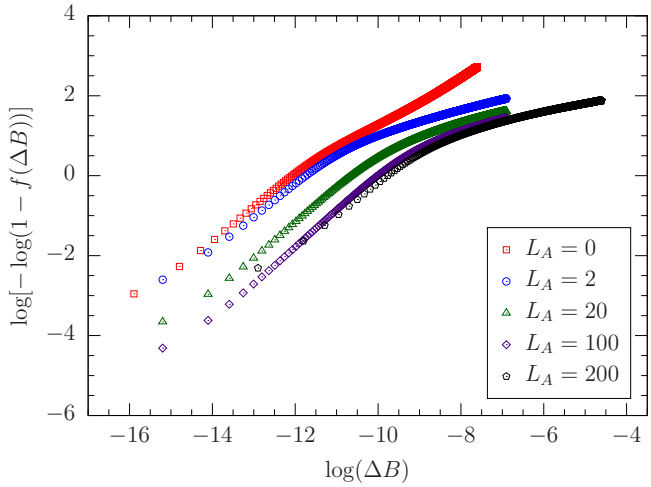

FIG. 17. Cumulative distribution of the interevent times for the RFIM across an internal hysteresis loop, which exhibits return point memory for $R = 2.3$ and $N = 200^3$. The data are more linear in a log-log plot for $L_A = 0$ than $L_A = 2$. Both ΔA and ΔF are similar to the results for the whole hysteresis loop.

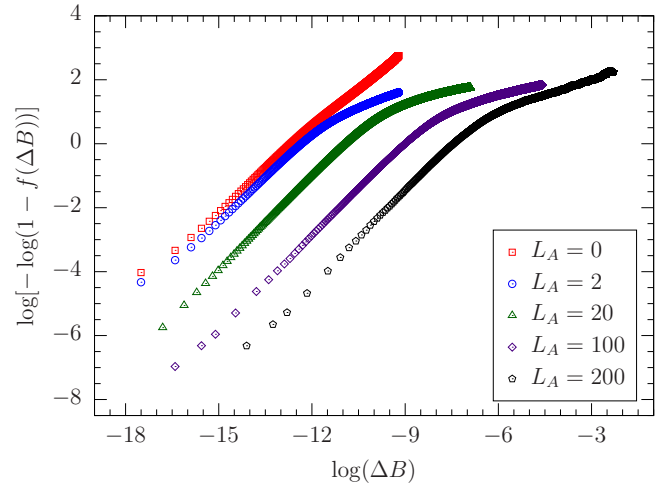

FIG. 18. Cumulative distribution of the interevent times for the RFIM across an internal hysteresis loop, which exhibits return point memory for $R = 3$ and $N = 200^3$. The data are Weibull distributed for $L_A = 0$.

same as in the one-dimensional case [17]. By examining the dependence of the interevent distribution on the disorder, one finds nonmonotonic behavior where $C(R)$ [Eq. (9)] peaks at $\sim$3.7, similar to the one-dimensional case.

Regarding the second point, we have added a large avalanche threshold, similar to the large earthquake threshold used in geophysics [34]. This leads to a distribution of interevent times for several methods of counting time. Counting the number of individual spin flips, counting the small avalanches, and the original measurement in terms of the change in magnetic field. We see no evidence for a sharpening of the interevent time distribution function which would be a confirmation that large events occur at a specific ΔA or ΔF. The clock-time fit to a Weibull distribution, however, is improved by the introduction of an event threshold L_A (Fig. 11) in the SKM. The distribution of the natural time ΔA can also be fit to a Weibull distribution in the SKM (Fig. 12).

Finally, we applied the same analysis to interevent distributions for a model system with added small-world bonds, i.e., bonds between random pairs of lattice sites. As the strength of these small-world bonds is increased, there are fewer small interevent times and fewer small avalanches. This is due to the increased correlation of lattice sites. As the correlation increases, avalanches coalesce into large avalanches, which reduces the number of small interevent times and small avalanche sizes. In some sense, the strength of the long-range bonds could be thought of as a tuning parameter between the distribution of avalanche sizes and interevent times.

By adding the long-range bonds to the lattice, the interevent distributions of large avalanches do not change. There is one main difference when long-range bonds are added. Namely, the value of the critical disorder increases when the strength of the long-range interactions are increased. As long as the disorder relative to the critical region is the same, the statistics of large avalanche interevent times is the same for any strength of the long-range interactions. Thus this modification of the model to make natural time a more effective clock is seen not to be effective.

There are several possible objectives to a quantitative evaluation of interevent times. One goal is a determination of their distribution function. In such an investigation, it is possible that alternate definitions of time, ΔB, ΔA, or ΔF in the work reported here, might lead to more simple or well understood distributions. We have shown that in the SKM, the use of a finite event threshold and ΔA simplifies the nature of $P(\Delta A)$ to a Weibull distribution.

A second goal concerns the *prediction* of the next (large) event. That requires not only finding the distribution function, but also, through the use of an appropriate redefinition of time, acquiring a distribution function which is sharply peaked, so the separation between events is known. This is, obviously, a holy grail for earthquake prediction. We have not succeeded in finding such a transformation for interacting spin models. Nevertheless, we suggest that further exploring the idea within simple models might be a useful, more controllable, complement to analysis of observational data.

ACKNOWLEDGMENTS

We thank Alexis Giguere, Molly Luginbuhl, John Rundle, and Don Turcotte for discussions on geophysics, Mario D'Andrea for initial coding, discussion, and writing, Juan Carlos Andresen for sharing base software, and Texas A&M University for access to their HPC resources. H.G.K. would like to thank Mezcal Reposado for motivation during the final stages of the manuscript. The work of R.S. and J.F. was supported by the Department of Energy, Grant No. DE-SC0014671. H.G.K. and A.B. acknowledge support from the NSF (Grant No. DMR-1151387). H.G.K.'s research is based upon work supported by the Office of the Director of National Intelligence (ODNI), Intelligence Advanced Research Projects Activity (IARPA), via Interagency Umbrella Agreement No. IA1-1198. The views and conclusions contained

herein are those of the authors and should not be interpreted as necessarily representing the official policies or endorsements, either expressed or implied, of the ODNI, IARPA, or the U.S. Government. The U.S. Government is authorized to reproduce and distribute reprints for Governmental purposes notwithstanding any copyright annotation thereon.

[1] W. Klein, J. B. Rundle, and C. D. Ferguson, Scaling and Nucleation in Models of Earthquake Faults, Phys. Rev. Lett. **78**, 3793 (1997).
[2] L. I. Salminen, A. I. Tolvanen, and M. J. Alava, Acoustic Emission from Paper Fracture, Phys. Rev. Lett. **89**, 185503 (2002).
[3] B. B. Goodman, Type II superconductors, Rep. Prog. Phys. **29**, 445 (1966).
[4] I. D. Mayergoyz, Mathematical Models of Hysteresis, Phys. Rev. Lett. **56**, 1518 (1986).
[5] I. D. Mayergoyz, *Mathematical Models of Hysteresis* (Springer, New York, 1991).
[6] J. B. Rundle, D. L. Turcotte, A. Donnellan, L. Grant Ludwig, M. Luginbuhl, and G. Gong, Nowcasting earthquakes, Earth and Space Science **3**, 480 (2016).
[7] P. A. Varotsos, N. V. Sarlis, H. K. Tanaka, and E. S. Skordas, Some properties of the entropy in the natural time, Phys. Rev. E **71**, 032102 (2005).
[8] P. A. Varotsos, N. V. Sarlis, and E. S. Skordas, *Natural Time Analysis: The New View of Time* (Springer, Berlin, 2011).
[9] J. B. Rundle, M. Luginbuhl, A. Giguere, and D. L. Turcotte, *Natural Time, Nowcasting and the Physics of Earthquakes: Estimation of Seismic Risk to Global Megacities* (Springer International Publishing, Cham, 2019), p. 123.
[10] D. S. Fisher and D. A. Huse, Absence of many states in realistic spin glasses, J. Phys. A **20**, L1005 (1987).
[11] A. J. Bray and M. A. Moore, Scaling theory of the ordered phase of spin glasses, in *Heidelberg Colloquium on Glassy Dynamics and Optimization*, edited by L. Van Hemmen and I. Morgenstern (Springer, New York, 1986), p. 121.
[12] W. L. McMillan, Scaling theory of Ising spin glasses, J. Phys. C **17**, 3179 (1984).
[13] C. M. Newman and D. L. Stein, Multiple states and thermodynamic limits in short-ranged Ising spin-glass models, Phys. Rev. B **46**, 973 (1992).
[14] G. Parisi, Infinite Number of Order Parameters for Spin-Glasses, Phys. Rev. Lett. **43**, 1754 (1979).
[15] M. Mézard, G. Parisi, and M. A. Virasoro, *Spin Glass Theory and Beyond* (World Scientific, Singapore, 1987).
[16] K. Binder and A. P. Young, Spin glasses: Experimental facts, theoretical concepts and open questions, Rev. Mod. Phys. **58**, 801 (1986).
[17] J. N. Nampoothiri, K. Ramola, S. Sabhapandit, and B. Chakraborty, Gaps between avalanches in one-dimensional random-field Ising models, Phys. Rev. E **96**, 032107 (2017).
[18] J. Lin, A. Saade, E. Lerner, A. Rosso, and M. Wyart, On the density of shear transformations in amorphous solids, Eur. Phys. Lett. **105**, 26003 (2014).
[19] S. Karmakar, E. Lerner, and I. Procaccia, Statistical physics of the yielding transition in amorphous solids, Phys. Rev. E **82**, 055103 (2010).
[20] M. Müller and M. Wyart, Marginal stability in structural, spin, and electron glasses, Annu. Rev. Condens. Matter Phys. **6**, 177 (2015).
[21] J. Lin, E. Lerner, A. Rosso, and M. Wyart, Scaling description of the yielding transition in soft amorphous solids at zero temperature, Proc. Natl. Acad. Sci. USA **111**, 14382 (2014).
[22] M. Wyart, Marginal Stability Constrains Force and Pair Distributions at Random Close Packing, Phys. Rev. Lett. **109**, 125502 (2012).
[23] T. Nattermann, Dipolar interaction in random-field systems, J. Phys. A **21**, L645 (1988).
[24] D. P. Belanger, Random-field experiments in dilute antiferromagnets, Phase Trans. **11**, 53 (1988).
[25] D. P. Belanger and A. P. Young, The random field Ising model, J. Magn. Magn. Mater. **100**, 272 (1991).
[26] H. Rieger, Monte Carlo studies of Ising spin glasses and random field systems, in *Annual Reviews of Computational Physics II* (World Scientific, Singapore, 1995), pp. 295–341.
[27] T. Nattermann, Theory of the random field Ising model, in *Spin Glasses and Random Fields*, edited by A. P. Young (World Scientific, Singapore, 1998), p. 277.
[28] O. Perkovic, K. A. Dahmen, and J. P. Sethna, Avalanches, Barkhausen Noise, and Plain Old Criticality, Phys. Rev. Lett. **75**, 4528 (1995).
[29] D. Sherrington and S. Kirkpatrick, Solvable Model of a Spin Glass, Phys. Rev. Lett. **35**, 1792 (1975).
[30] J. C. Andresen, Z. Zhu, R. S. Andrist, H. G. Katzgraber, V. Dobrosavljević, and G. T. Zimanyi, Self-Organized Criticality in Glassy Spin Systems Requires a Diverging Number of Neighbors, Phys. Rev. Lett. **111**, 097203 (2013).
[31] A. Sharma, J. Yeo, and M. A. Moore, Self-organized critical behavior and marginality in Ising spin glasses, J. Stat. Mech. (2018) 053302.
[32] L. Viana and A. J. Bray, Phase diagrams for dilute spin glasses, J. Phys. C **18**, 3037 (1985).
[33] S. Schnabel and W. Janke, Dynamic greedy algorithms for the Edwards-Anderson model, Comput. Phys. Commun. **220**, 74 (2017).
[34] P. A. Varotsos, N. V. Sarlis, E. S. Skordas, H. K. Tanaka, and M. S. Lazaridou, Attempt to distinguish long-range temporal correlations from the statistics of the increments by natural time analysis, Phys. Rev. E **74**, 021123 (2006).
[35] F. Pázmándi, G. Zaránd, and G. T. Zimányi, Self-Organized Criticality in the Hysteresis of the Sherrington-Kirkpatrick Model, Phys. Rev. Lett. **83**, 1034 (1999).
[36] Z. Zhu, J. C. Andresen, M. A. Moore, and H. G. Katzgraber, Boolean decision problems with competing interactions on scale-free networks: Equilibrium and nonequilibrium behavior in an external bias, Phys. Rev. E **89**, 022118 (2014).
[37] A. Sharma, A. Andreanov, and M. Müller, Avalanches and hysteresis in frustrated superconductors and XY spin glasses, Phys. Rev. E **90**, 042103 (2014).
[38] O. S. Sarıyer, A. Kabakcioglu, and A. N. Berker, Deep Spin-Glass Hysteresis Area Collapse and Scaling in the $d = 3 \pm J$ Ising Model, Phys. Rev. E **86**, 041107 (2012).
[39] R. Bruinsma and G. Aeppli, Interface Motion and Nonequilibrium Properties of the Random-Field Ising Model, Phys. Rev. Lett. **52**, 1547 (1984).

[40] R. T. Scalettar, Critical properties of an Ising model with dilute long range interactions, Physica A **170**, 282 (1991).

[41] R. Albert and A.-L. Barabási, Statistical mechanics of complex networks, Rev. Mod. Phys. **74**, 47 (2002).

[42] H. G. Katzgraber, F. Pázmándi, C. R. Pike, K. Liu, R. T. Scalettar, K. L. Verosub, and G. T. Zimányi, Reversal-Field Memory in the Hysteresis of Spin Glasses, Phys. Rev. Lett. **89**, 257202 (2002).

[43] J. P. Sethna, K. Dahmen, S. Kartha, J. A. Krumhansl, B. W. Roberts, and J. D. Shore, Hysteresis and Hierarchies: Dynamics of Disorder-Driven First-Order Phase Transformations, Phys. Rev. Lett. **70**, 3347 (1993).

[44] J. M. Deutsch, A. Dhar, and O. Narayan, Return to Return Point Memory, Phys. Rev. Lett. **92**, 227203 (2004).